98-24

Research report. A numerical study of the solution to the 3D incompressible Navier-Stokes equations

Heinz-Otto Kreiss*
(email: kreiss@math.ucla.edu)
&
Jacob Ystrom*
(email: jystrom@math.ucla.edu)

Department of Mathematics, UCLA
Los Angeles, CA 90024

April 15, 1998

Abstract

This report describes three series of numerical experiments for the three-dimensional incompressible Navier-Stokes equations. In the first experiment the smallest scale estimate $\lambda_{min} = \sqrt{\nu/|D\boldsymbol{u}|_\infty}$ is studied. It is demonstrated that the estimate is sharp and that if the smallest scale is well resolved the numerical approximations on different grids converge in the max-norm. In the second experiment a high frequency perturbation is considered. We show that coherent structures are quite stable to perturbations. On a short time-scale high frequency perturbations are effectively damped. In the third experiment we demonstrate that the time history of the large scale (low Fourier modes) of the solution generate the small scale (high Fourier modes).

*Supported by the office of Naval research grant no. N00014-93-1-0551; P00005 and no. N00014-98-1-0125

Contents

1 Introduction

In this report we summarize some results for the numerical solution of the three-dimensional incompressible Navier-Stokes equations,

$$\boldsymbol{u}_t + (\boldsymbol{u}\cdot\nabla)\boldsymbol{u} + \nabla p = \nu\Delta\boldsymbol{u}, \quad \nu > 0, \tag{1.1a}$$

$$\nabla\cdot\boldsymbol{u} = 0, \tag{1.1b}$$

with 2π-periodic boundary conditions. We can expand the solution into Fourier series

$$\boldsymbol{u}(\boldsymbol{x},t) = \sum_{\boldsymbol{k}} \hat{\boldsymbol{u}}(\boldsymbol{k},t)e^{i\boldsymbol{k}^T\cdot\boldsymbol{x}}, \tag{1.2}$$

$$p(\boldsymbol{x},t) = \sum_{\boldsymbol{k}} \hat{p}(\boldsymbol{k},t)e^{i\boldsymbol{k}^T\cdot\boldsymbol{x}}, \tag{1.3}$$

where $\boldsymbol{x} = (x,y,z)^T$, $\boldsymbol{u} = (u,v,w)^T$ and $\boldsymbol{k} = (k_1,k_2,k_3)^T$, $k_i \in \mathcal{N}$. As usual we define the kinetic energy spectrum,

$$E(k) = \frac{1}{2}\sum_{k-1/2\le|\boldsymbol{k}|<k+1/2} |\hat{\boldsymbol{u}}(\boldsymbol{k},t)|^2.$$

Thus

$$\begin{aligned} \|\boldsymbol{u}\|^2 &= V\sum_{\boldsymbol{k}} |\hat{\boldsymbol{u}}(\boldsymbol{k},t)|^2 \\ &= V\sum_{k}\Big(\sum_{k-1/2\le|\boldsymbol{k}|<k+1/2} |\hat{\boldsymbol{u}}(\boldsymbol{k},t)|^2\Big) \\ &= 2V\sum_{k} E(k), \end{aligned}$$

where $V = (2\pi)^3$. To solve the equations we use in space the pseudo-spectral method with de-aliasing and for the time marching, we use the second order Adams-Bashforth method in combination with the Crank-Nicolson for the viscous terms. The calculations are of relaxation type, i.e. the initial data evolve freely and no outer forcing is imposed. The initial data

$$\boldsymbol{u}(\boldsymbol{x},0) = \boldsymbol{u}_0(\boldsymbol{x}), \quad p(\boldsymbol{x},0) = p_0(\boldsymbol{x}),$$

are chosen to have a prescribed spectrum with a random phase, satisfying the incompressibility constraint (1.1b).

For the same initial data we make two base-runs on a grid with $N = 256$ grid points in each space direction. The only difference between the two calculations is the value of the viscosity, $\nu = 1/153, 1/300$ respectively. In section 3 we make a comparison between these calculations.

In section 4 the base-run with larger viscosity is used as reference for calculations on coarser grids with $N = 64$ and 128 grid points respectively. Based on the smallest scale estimate [1], the data are such that the solution is not resolved when $N = 64$, but resolved on the finer grid, where $N = 128$. As expected the solution on the coarser grid deviates significantly from the reference solution while the solution on the finer grid is close to the reference solution.

In section 5 we use the base-run with the smaller viscosity as a reference solution for two perturbation calculations. A rather large high mode perturbation of the base-run is made at $t = 0.5$. At this time, the spectrum shape has stabilized. At the beginning the difference between the base-run and the perturbed solution decays rapidly which means that the coherent structures are stable to high mode perturbations. After a while the difference starts to increase. We believe that, as in two-space dimensions c.f. [2], after some time the effect of the perturbation is pushed into the low modes and the solutions start to deviate.

In section 6 we demonstrate that the time history of the large scales of the solution can actually generate its own small scale. Perhaps surprisingly, we obtain the same results as in two space dimensions c.f. [3]. We use the base-run with $\nu = 1/300$ as a reference solution. Let k_c be a natural number. We denote base-run-2 by $\boldsymbol{u}_b(\boldsymbol{x}, t)$ and write it in the form

$$\boldsymbol{u}_b = \boldsymbol{u}_b^I + \boldsymbol{u}_b^{II},$$

where

$$\boldsymbol{u}_b^I = \boldsymbol{u}_b^I(\boldsymbol{x}, t) = \sum_{|\boldsymbol{k}| \le k_c + 1/2} \hat{\boldsymbol{u}}(\boldsymbol{k}, t) e^{i\boldsymbol{k}^T \cdot \boldsymbol{x}}, \quad \boldsymbol{u}_b^{II} = \boldsymbol{u}_b - \boldsymbol{u}_b^I.$$

We call $\boldsymbol{u}_b^I$ the large scale and $\boldsymbol{u}_b^{II}$ the small scale. We make the following two types of experiments.

1. At time $t = 0.5$ we restart the calculations by truncating $\boldsymbol{u}_b$ to $\boldsymbol{u}_b^I$, i.e. we restart the calculations at $t = 0.5$ with initial data

   $$\boldsymbol{u}^I(\boldsymbol{x}, 0.5) = \boldsymbol{u}_b^I(\boldsymbol{x}, 0.5), \quad \boldsymbol{u}^{II}(\boldsymbol{x}, 0.5) = 0. \tag{1.4}$$

   We call the new solution truncated run and denote it by $\boldsymbol{u}_T$.

2. We restart the calculations at $t = 0.5$ with the truncated data (1.4) and force the solution at every time step by $\boldsymbol{u}_b^I(\boldsymbol{x}, t)$ i.e. we replace at every time step $\boldsymbol{u}^I$ by $\boldsymbol{u}_b^I$. We call the solution playback run and denote it by $\boldsymbol{u}_{pb}$. Clearly $\boldsymbol{u}_{pb}^I(\boldsymbol{x}, t) = \boldsymbol{u}_b^I(\boldsymbol{x}, t)$.

Mathematically we can express the Navier-Stokes equations (1.1) in the following way, for the large scale

$$\begin{aligned} &\boldsymbol{u}_t^I + (((\boldsymbol{u}^I + \boldsymbol{u}^{II}) \cdot \nabla)\boldsymbol{u}^I)^I + \\ &\quad ((\boldsymbol{u}^I \cdot \nabla)\boldsymbol{u}^{II})^I + \nabla p^I = \nu \Delta \boldsymbol{u}^I + F^I(\boldsymbol{u}^{II}), && \text{(1.5a)} \\ &\quad \nabla \cdot \boldsymbol{u}^I = 0, && \text{(1.5b)} \end{aligned}$$

and for the small scale

$$\begin{aligned} &\boldsymbol{u}_t^{II} + (((\boldsymbol{u}^I + \boldsymbol{u}^{II}) \cdot \nabla)\boldsymbol{u}^{II})^{II} + \\ &\quad ((\boldsymbol{u}^{II} \cdot \nabla)\boldsymbol{u}^I)^{II} + \nabla p^{II} = \nu \Delta \boldsymbol{u}^{II} + F^{II}(\boldsymbol{u}^I), && \text{(1.6a)} \\ &\quad \nabla \cdot \boldsymbol{u}^{II} = 0, && \text{(1.6b)} \end{aligned}$$

where

$$\begin{aligned} F^I(\boldsymbol{u}^{II}) &= -((\boldsymbol{u}^{II} \cdot \nabla)\boldsymbol{u}^{II})^I, \\ F^{II}(\boldsymbol{u}^I) &= -((\boldsymbol{u}^I \cdot \nabla)\boldsymbol{u}^I)^{II}. \end{aligned}$$

The type 2) experiment above can be formulated as;
find the solution $\boldsymbol{u}^{II}(\boldsymbol{x},t), t \geq 0.5$ to equations (1.6) with

$$\boldsymbol{u}^{I}(\boldsymbol{x},t) = \boldsymbol{u}_b^{I}(\boldsymbol{x},t),$$

and with initial data,

$$\boldsymbol{u}^{II}(\boldsymbol{x},0.5) = 0.$$

We say that the large scale reproduces the small scale $\boldsymbol{u}_b^{II}(\boldsymbol{x},t)$ if

$$\boldsymbol{u}_b^{II}(\boldsymbol{x},t) - \boldsymbol{u}_{pb}^{II}(\boldsymbol{x},t) \rightarrow 0.$$

2 Numerical technique

The experiments in this report uses a spectral DNS (Direct Numerical Simulation) computer program which is based on a program from the Department of Mechanics at the Royal Institute of Technology, Stockholm Sweden. Several authors have contributed to the code c.f. [4],[5],[6]. The program utilizes a spectral formulation that practically means that on the spectral side only two ODE's, for the y components of the velocity and vorticity, have to be solved for each $\boldsymbol{k}$. The reason is that the pressure p can on the spectral side completely be eliminated and that the continuity equation and the vorticity definition are simple algebraic relations for the velocity components from which the x and z components can be updated at each time step.

2.1 Space discretization

In space, the pseudo-spectral method with de-aliasing is used. We only consider equal grid spacing in all directions. Let e.g. $N = 2^j$ for some $j > 0$, and

$$k_i \in [-N/2+1, N/2], \quad i = 1,2,3.$$

We denote the smallest scale that we can represent on the grid by λ_{min}^{G} and will use the relation

$$\lambda_{min}^{G} = 1/k_{max} = 2/N.$$

The FFT algorithm is used to go between spectral and physical space. The FFT routines used are optimized specially for vector machines. Furthermore the FFT subroutine calls can be made in parallel. The 3D FFT is done plane by plane, each plane transformed independently of other parallel planes.

2.2 Time discretization

The non-linear terms are treated explicitly with a second order Adams-Bashforth method. The linear viscous term is computed with help of the second order Crank-Nicolson method. There is a variable time step feature implemented in the code but since we want to do comparisons between different calculations at equal simulation times, we choose to use a constant time step.

2.3 Numerical solutions

By a numerical solution we mean the Fourier polynomial,

$$\boldsymbol{u}(\boldsymbol{x}, t_n) = \sum_{k_1=-N/2+1}^{N/2} \sum_{k_2=-N/2+1}^{N/2} \sum_{k_3=-N/2+1}^{N/2} \tilde{\boldsymbol{u}}(\boldsymbol{k}, t_n) e^{i\boldsymbol{k}^T \cdot \boldsymbol{x}},$$

where the $\tilde{\boldsymbol{u}}(\boldsymbol{k}, t_n)$ are obtained from the numerical algorithm. As usual the vorticity is defined by,

$$\boldsymbol{\xi} = (\xi^x, \xi^y, \xi^z)^T = \nabla \times \boldsymbol{u} = (w_y - v_z, u_z - w_x, v_x - u_y)^T.$$

2.4 Norms

We denote the L_2 norm over the whole 3D domain by,

$$|||\boldsymbol{u}|||^2 = \int_0^{2\pi} \int_0^{2\pi} \int_0^{2\pi} |\boldsymbol{u}|^2 \, \mathrm{d}x\mathrm{d}y\mathrm{d}z,$$

and the L_2 norm over a $y = const.$ plane by,

$$||\boldsymbol{u}||^2 = \int_0^{2\pi} \int_0^{2\pi} |\boldsymbol{u}|^2 \, \mathrm{d}x\mathrm{d}z.$$

3 Base-runs

In this section we present two calculations, base-run-1 and base-run-2 which differ only in the viscosity. The viscosity in base-run-1 is $\nu = 1/153$ and

in base-run-2, $\nu = 1/300$. In section 4, base-run-1 is used for reference in a series of grid-refinement computation. In section 5 and 6, base-run-2 is used for reference for high-mode perturbations and for low-mode forcing respectively. The initial data for the base runs are constructed with random phase distribution, satisfying the incompressibility constraint,

$$\nabla \cdot \boldsymbol{u} = 0,$$

and with the spectrum,

$$E_b(k) = C_b k e^{-(k/k_0)^2},$$

where $k_0 = 3.76$ and C_b is 5 such that

$$\frac{1}{2V}|||\boldsymbol{u}(\boldsymbol{x}, 0)|||^2 = 0.5.$$

Since the presentation and comparison of 3D data is practically difficult we will restrict the comparison and plotting to the y component of the vorticity, ξ^y in planes for which $y = const.$ We argue that the solution is isotropic and therefore, that our conclusions are also valid for the whole solution, c.f. figure 1 where,

$$\alpha_i = \frac{\sum_{\boldsymbol{k}} |\tilde{\xi}^i|^2}{\sum_{\boldsymbol{k}} |\tilde{\boldsymbol{\xi}}|^2} - \frac{1}{3}, \quad i = x, y, z,$$

a measure of the vorticity anisotropy for the base-run2 vs. time is plotted. In this section and in section 4 we use the plane $y = \pi$ for comparison and in section 5 and 6 the plane for which $|\xi_b^y|$ attains its maximum.

Contour plots of the initial data for base-run (1 and 2) can be seen in figure 2 (the y-vorticity for $y = \pi$). Positive vorticity is displayed with red and negative with blue. In figure 3 the two base-runs are compared at $t = 0.46$ and in figure 4 at $t = 0.91$.

In figure 5 and figure 6 some scalar quantities of the base-runs are monitored as time goes, $t \in [0, 1.0]$ for base-run-1 and $t \in [0, 4.5]$ for base-run-2. The kinetic energy per unit volume, rate of dissipation per unit volume is displayed as well as the global maximum of $|\xi^y|$.

In section 5 and section 6 we use the base-run-2 at $t = 0.5$ as initial data for a series of experiments. This is to get more physically reasonable initial data. At this time the spectrum shape is relatively stable.

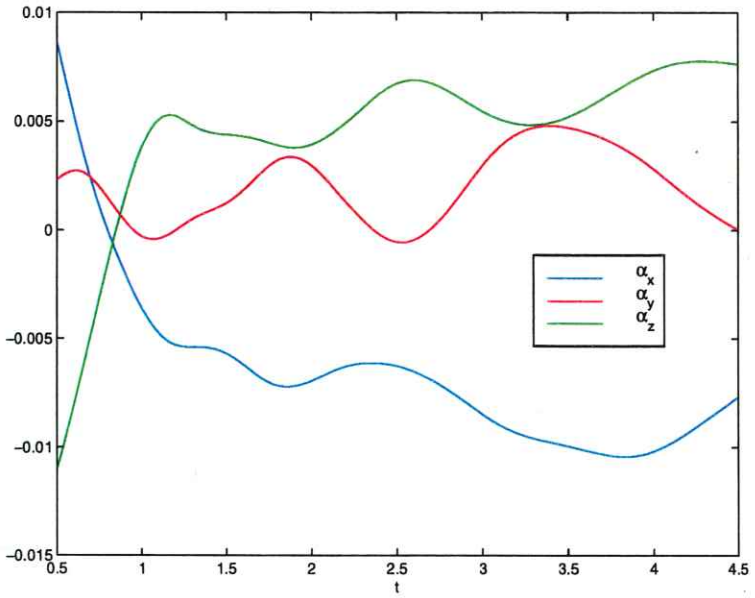

Figure 1: Anisotropy for the vorticity components, base-run-2

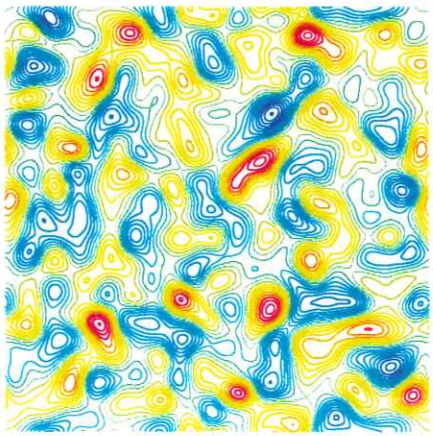

Figure 2: Initial data for base runs: ξ^y for $y = \pi, t = 0.0$. Contour spacing:1, (min,max): $(-10.1, 10.4)$

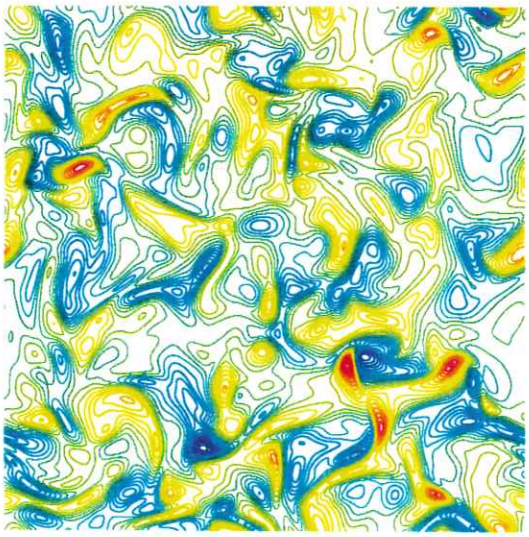

(a) (min,max): $(-15.7, 16.2)$

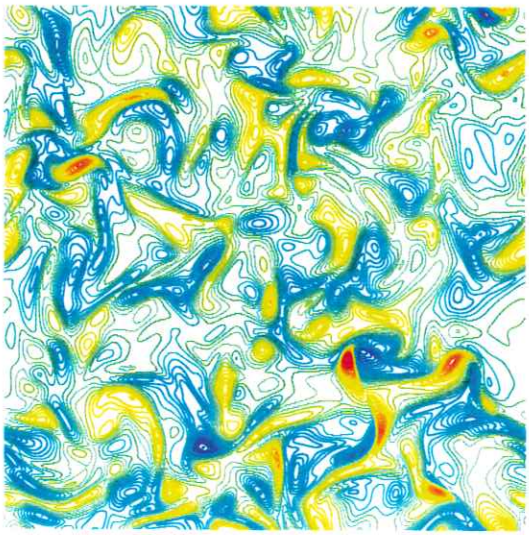

(b) (min,max): $(-18.1, 21.3)$

Figure 3: Contour plots of the y component of the vorticity, base-run-1 (a) and base-run-2 (b), $t = 0.46, y = \pi$. Contour spacing:1

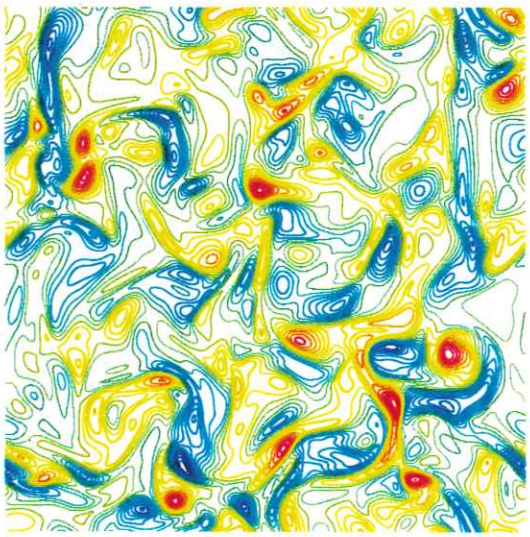

(a) (min,max): $(-12.9, 12.9)$

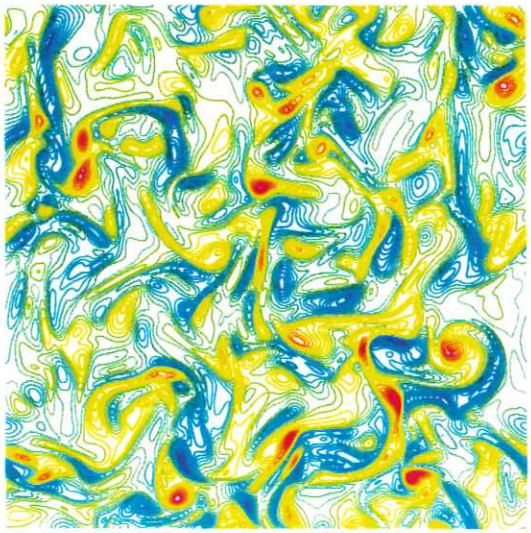

(b) (min,max): $(-19.2, 19.6)$

Figure 4: Contour plots of the y component of the vorticity, base-run-1 (a) and base-run-2 (b), $t = 0.91, y = \pi$. Contour spacing:1

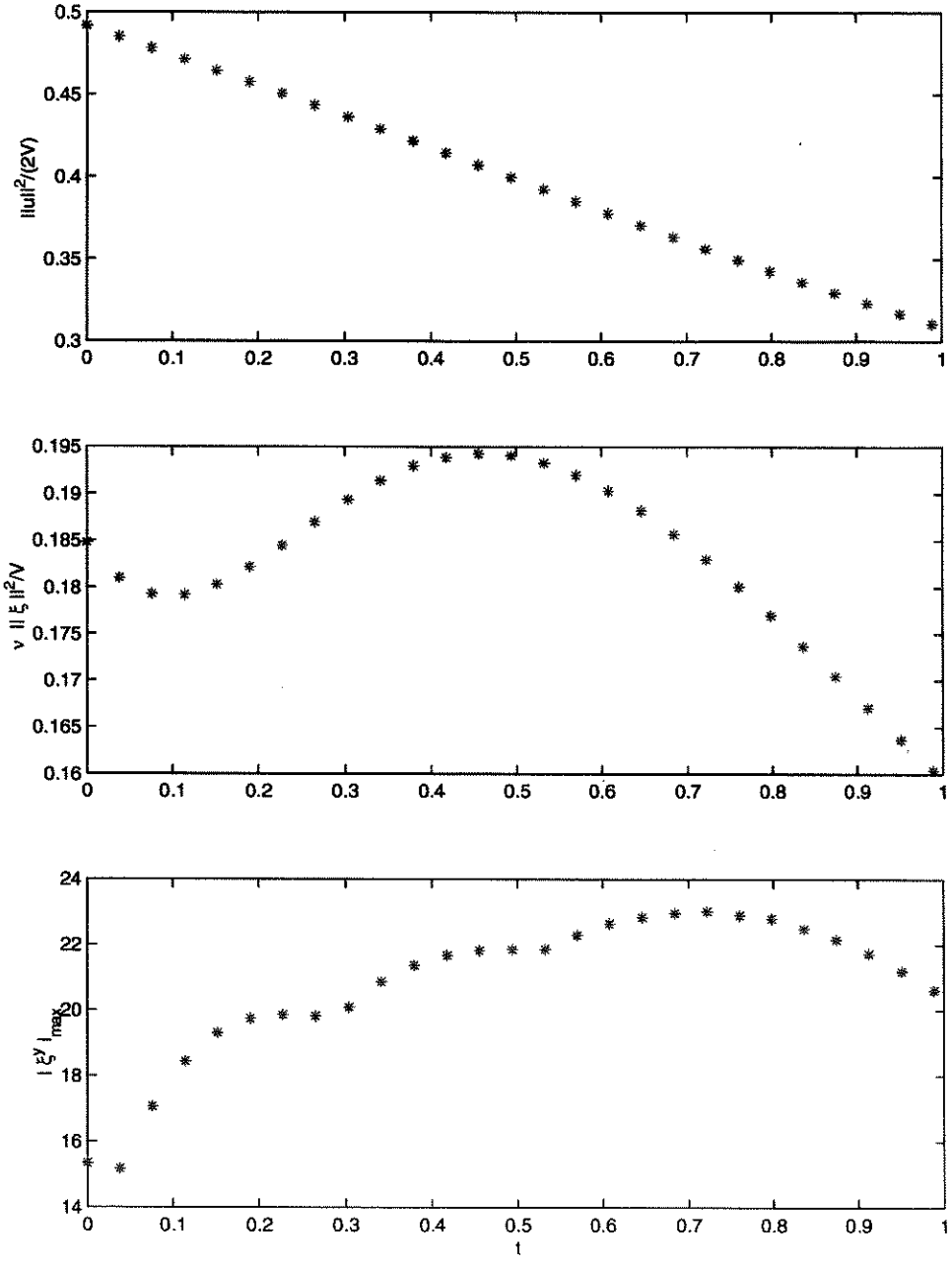

Figure 5: base-run-1: kinetic energy per unit volume, rate of dissipation per unit volume and $|\xi^y|_\infty$

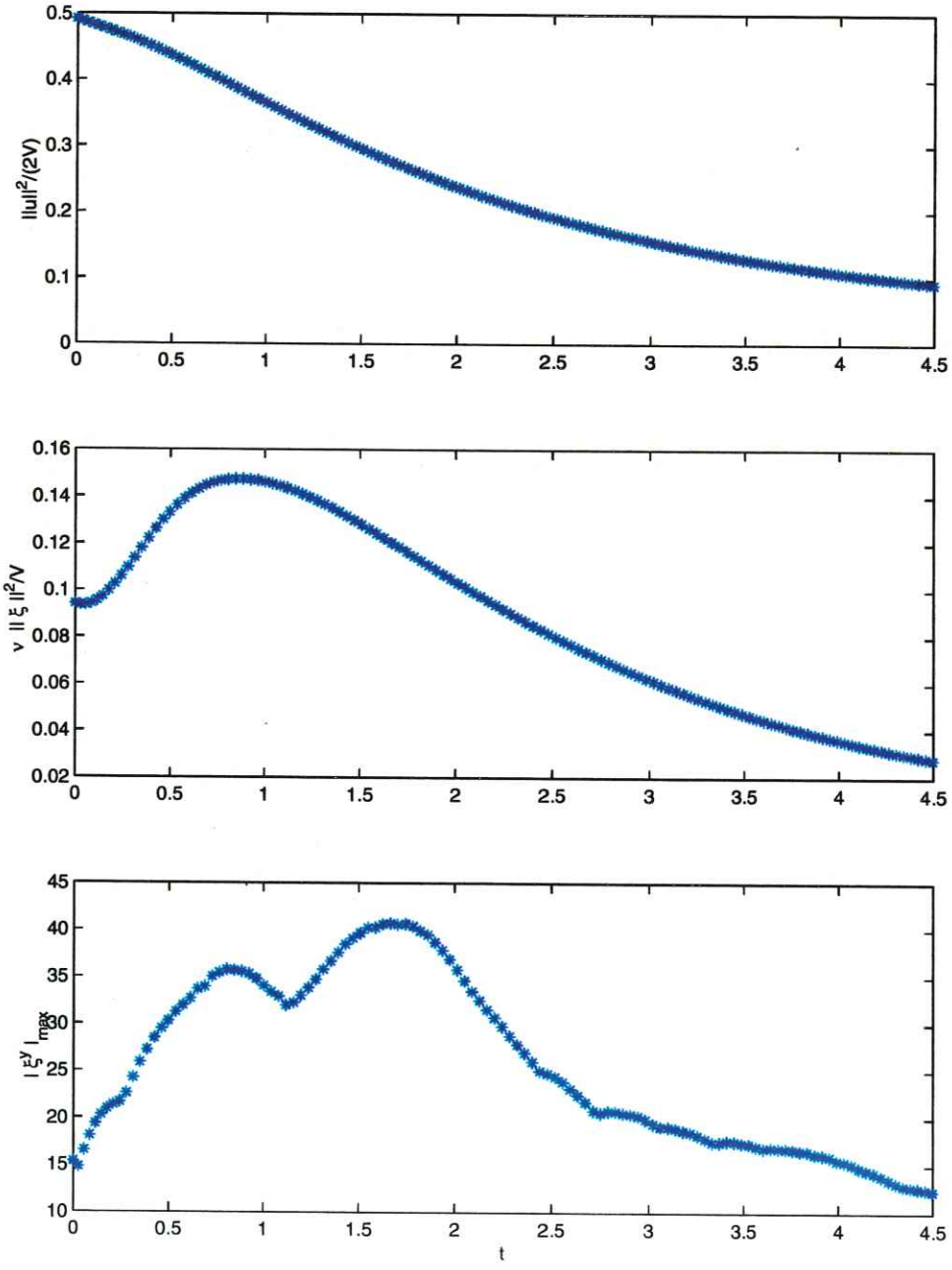

Figure 6: base-run-2: kinetic energy per unit volume, rate of dissipation per unit volume and $|\xi^y|_\infty$

4 Smallest scale and resolution requirement

In this section we investigate the need of spatial resolution and its influence on accuracy. In this context the smallest scale estimate, c.f. [1] is central. It states that the smallest length scale of the solution to eq. (1.1) is no smaller than,

$$\lambda_{min} \cong \sqrt{\frac{\nu}{\overline{|D\boldsymbol{u}|_\infty}}}$$

where

$$\overline{|D\boldsymbol{u}|_\infty} = \sup_t |D\boldsymbol{u}|_\infty = \sup_t \max_{\boldsymbol{x},i} |\nabla u_i|.$$

In three space dimensions there is no a priori bound on $\overline{|D\boldsymbol{u}|_\infty}$, so the question of resolution requirement can strictly speaking not be determined beforehand. However, for the same initial data (and without outer forcing) the behavior

$$\overline{|D\boldsymbol{u}|_\infty} \sim \nu^{-1/2},$$

is typical. Consider the base-runs in the previous section. Instead of computing

$$\max_{\boldsymbol{x},i} |\nabla u_i|$$

for these runs, we compute

$$|\xi^y|_\infty = \max_{\boldsymbol{x}} |\xi^y|, \quad \overline{|\xi^y|_\infty} = \max_t |\xi^y|_\infty$$

and use

$$\lambda^*_{min} = \sqrt{\frac{\nu}{\overline{|\xi^y|_\infty}}},$$

as an estimate of the smallest scale. For the base-runs, the parameters in table 1 are obtained. The base-run-1 is very well resolved since

$$\lambda^*_{min}/\lambda^G_{min} = 2.2.$$

We now compute the numerical approximation on two grids with $N = 128, 64$ respectively for the same viscosity and time-step as for base-run-1, c.f. table 2, here the λ^*_{min} is taken from the base-run-1. Denote the vorticity of the different numerical solutions,

$$\boldsymbol{\xi}_N = \boldsymbol{\xi}_N(\boldsymbol{x}, t), \quad N = 256, 128, 64,$$

run	ν	N	Δt	λ^*_{min}	λ^G_{min}
base-run-1	0.0065	256	0.0019	0.0168	0.0078
base-run-2	0.0033	256	0.0019	0.0090	0.0078

Table 1: Parameters and data for base-runs.

and let $\boldsymbol{\xi} = \boldsymbol{\xi}(\boldsymbol{x}, t)$ denote the true solution. The relative L_2 norm error for the vorticity is approximated on the grids with $N = 128, 64$ as,

$$\begin{aligned}\frac{|||\boldsymbol{\xi}(\cdot,t) - \boldsymbol{\xi}_N(\cdot,t)|||}{|||\boldsymbol{\xi}(\cdot,t)|||} &\approx \frac{|||\boldsymbol{\xi}_{256}(\cdot,t) - \boldsymbol{\xi}_N(\cdot,t)|||}{|||\boldsymbol{\xi}_{256}(\cdot,t)|||} \\ &\approx \frac{|||\xi^y_{256}(\cdot,t) - \xi^y_N(\cdot,t)|||}{|||\xi^y_{256}(\cdot,t)|||} \\ &\approx \frac{\|\xi^y_{256}((\cdot,\pi,\cdot),t) - \xi^y_N((\cdot,\pi,\cdot),t)\|}{\|\xi^y_{256}((\cdot,\pi,\cdot),t)\|},\end{aligned}$$

i.e. the error is approximated as the error of the y component of the vorticity in a plane, $y = const.$. We approximate the relative max-norm error for the vorticity correspondingly. These approximations of the errors can be found in table 3. Observe that e.g. the Kolmogoroff length scale,

$$\lambda_{3D} = \nu^{3/4}/\epsilon^{1/4} > 0.035,$$

where ϵ is the rate of dissipation per unit volume c.f. figure 5. A smallest scale estimate based on the Kolmogoroff length scale implies that coarse grid should suffice to resolve the solution. This is clearly not the case c.f. table 3. For the calculation on the grid with $N = 128$ the relation

$$\lambda^*_{min}/\lambda^G_{min} = 1.1,$$

holds. This relation also holds for the the base-run-2. We therefore expect that the truncation errors for the base-run-2 are about the same as for $N = 128$, c.f. table 3.

5 High mode perturbation

In this section we consider a high mode perturbation of base-run-2. The perturbation is localized around a mode number k_0 in spectral space and is

grid	ν	N	Δt	λ^*_{min}	λ^G_{min}
very-fine	0.0065	256	0.0019	0.0168	0.0078
fine	0.0065	128	0.0019	0.0168	0.0156
coarse	0.0065	64	0.0019	0.0168	0.0312

Table 2: Parameters and data for grid-refinement calculations

N	t	y	$\frac{\|\xi^y_{256} - \xi^y_N\|}{\|\xi^y_{256}\|}$	$\frac{\|\xi^y_{256} - \xi^y_N\|_{max}}{\|\xi^y_{256}\|_{max}}$
64	0.000	π	0.000	0.000
64	0.152	π	0.016	0.066
64	0.304	π	0.052	0.134
64	0.456	π	0.071	0.102
64	0.608	π	0.084	0.142
64	0.760	π	0.088	0.115
64	0.912	π	0.081	0.112
128	0.000	π	0.000	0.000
128	0.152	π	0.0011	0.007
128	0.304	π	0.0046	0.016
128	0.456	π	0.0033	0.010
128	0.608	π	0.0033	0.0069
128	0.760	π	0.0036	0.0076
128	0.912	π	0.0027	0.0061

Table 3: Grid convergence in the plane $y = \pi$ for the y-component of vorticity.

added to the velocity components of the base-run-2, described in section 3, at $t = 0.5$. Denote the perturbed solution by $\boldsymbol{u}_{p,k_0}$ and denote the perturbation by $\boldsymbol{w}_{k_0}$. Now, let

$$\boldsymbol{u}_{p,k_0}(\boldsymbol{x}, 0.5) = \boldsymbol{u}_b(\boldsymbol{x}, 0.5) + \boldsymbol{w}_{k_0}(\boldsymbol{x}),$$

where the energy spectrum for $\boldsymbol{w}_{k_0}$ is of the form,

$$E_w(k) = C_w e^{-(k-k_0)^2}.$$

Let $\boldsymbol{\xi}_{k_0}$ denote the vorticity of the perturbation. C_w is chosen such that the enstrophy of the perturbation satisfies

$$\frac{1}{V}|||\boldsymbol{\xi}_{k_0}|||^2 = 18,$$

which can be compared to

$$\frac{1}{V}|||\boldsymbol{\xi}_b(\cdot, 0.5)|||^2 = 40.0.$$

The perturbation has random phase and fulfills the continuity equation,

$$\nabla \cdot \boldsymbol{w}_{k_0} = 0.$$

In figure 7 we plot the difference between the unperturbed and the perturbed solution in terms of the relative L_2 norm in $y = const.$ planes for $k_0 = 32, 64$. Here the planes are chosen such that $|\xi_b^y|$ attains its maximum in the plane. For practical purposes these maximum values and these planes are taken on a grid with $\frac{3}{2} * N$ points in each direction. We use the notation,

$$y_j = (j-1)h = (j-1)(4\pi/(3N)), \quad j = 1, ..., 3N/2.$$

The norms can also be found in table 5. Contour plots of $\xi_b^y, \xi_{p,32}^y$ are shown at the start of the simulation in figures 8, close to the time at which the difference attains its minimum(in L_2-norm) in figure 9 and at the end of the simulation in figure 10.

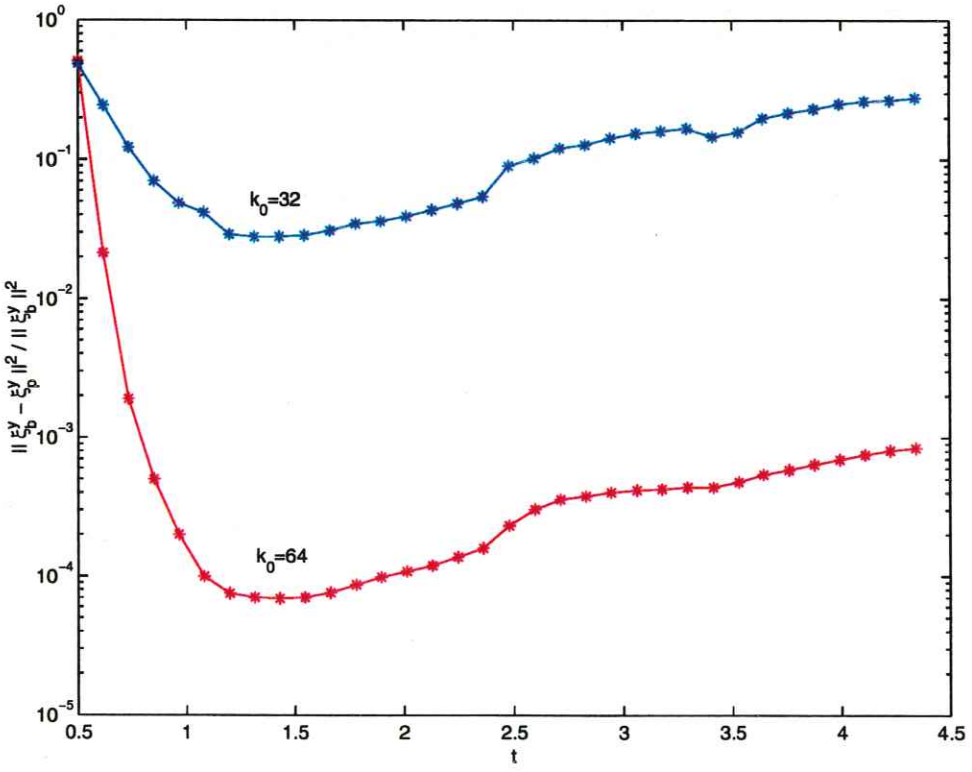

Figure 7: Difference between perturbed and unperturbed solution, $k_0 = 32, 64$.

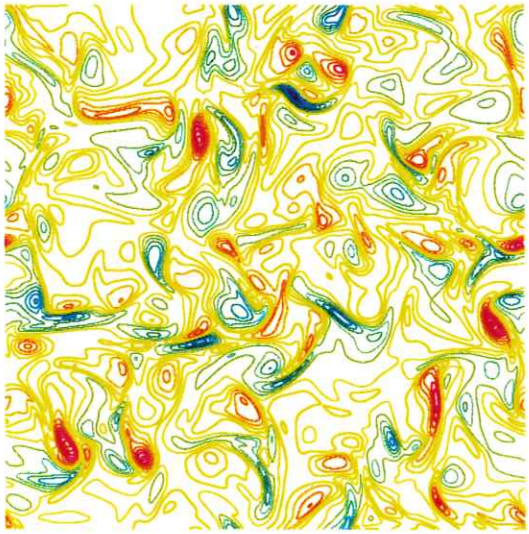

(a) (min,max): $(-30.3, 19.8)$

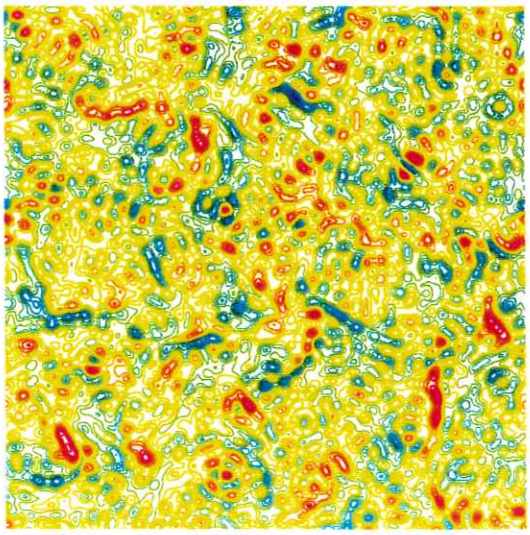

(b) (min,max): $(-31.3, 21.0)$

Figure 8: Base-run (a) and perturbed-run (b): $\xi^y, t = 0.5, k_0 = 32$. Contour spacing:2

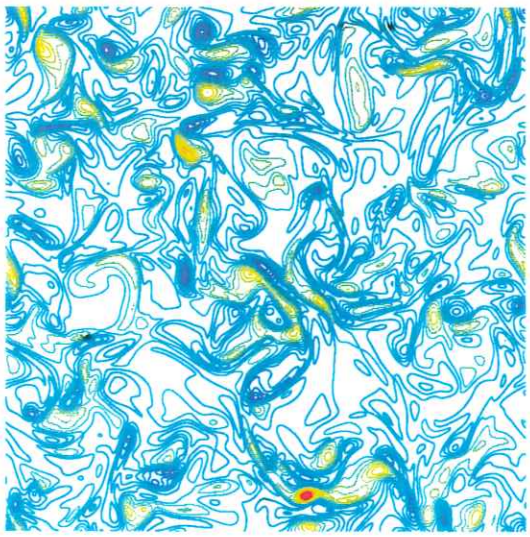

(a) (min,max): $(-19.2, 35.8)$

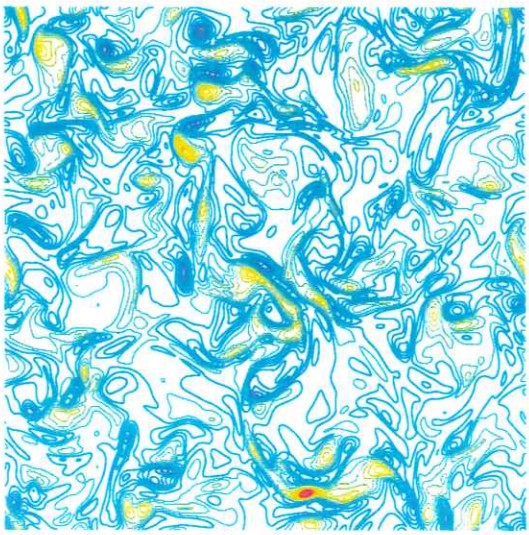

(b) (min,max): $(-20.0, 35.8)$

Figure 9: Base-run (a) and perturbed-run (b): $\xi^y, t = 1.32, k_0 = 32$. Contour spacing:2

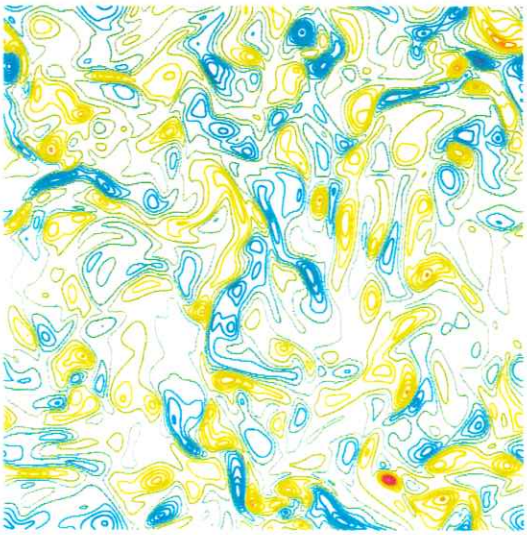

(a) (min,max): $(-12.0, 12.9)$

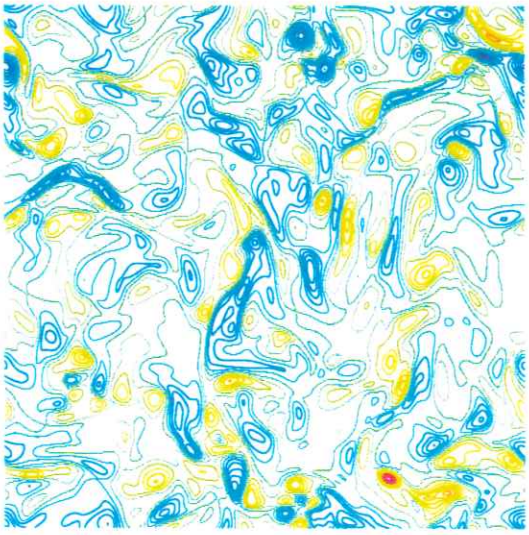

(b) (min,max): $(-10.4, 12.9)$

Figure 10: Base-run (a) and perturbed-run (b): $\xi^y, t = 4.34, k_0 = 32$. Contour spacing:1

t	y	$\frac{\|\xi_b^y - \xi_{p,k_0=32}^y\|^2}{\|\xi_b^y\|^2}$	$\frac{\|\xi_b^y - \xi_{p,k_0=64}^y\|^2}{\|\xi_b^y\|^2}$
0.5000	y_{264}	0.4889	0.5097
0.6164	y_{264}	0.2456	0.0214
0.7328	y_{263}	0.1226	0.0019
0.8492	y_{264}	0.0701	0.0005
0.9656	y_{263}	0.0489	0.0002
1.0820	y_{324}	0.0418	0.0001
1.1984	y_{190}	0.0291	0.000075
1.3148	y_{192}	0.0279	0.000071
1.4312	y_{193}	0.0280	0.000069
1.5476	y_{192}	0.0286	0.000070
1.6640	y_{192}	0.0310	0.000076
1.7804	y_{189}	0.0347	0.000087
1.8968	y_{189}	0.0363	0.00010
2.0132	y_{190}	0.0393	0.00011
2.1296	y_{192}	0.0435	0.00012
2.2460	y_{193}	0.0486	0.00014
2.3624	y_{193}	0.0545	0.00016
2.4788	y_{162}	0.0905	0.00023
2.5952	y_{159}	0.1028	0.00030
2.7116	y_{157}	0.1212	0.00036
2.8280	y_{153}	0.1282	0.00038
2.9444	y_{153}	0.1429	0.00040
3.0608	y_{152}	0.1548	0.00042
3.1772	y_{150}	0.1612	0.00043
3.2936	y_{149}	0.1681	0.00044
3.4100	y_{300}	0.1463	0.00044
3.5264	y_{301}	0.1580	0.00048
3.6428	y_{171}	0.1989	0.00054
3.7592	y_{171}	0.2171	0.00059
3.8756	y_{173}	0.2317	0.00064
3.9920	y_{173}	0.2511	0.00070
4.1084	y_{174}	0.2630	0.00075
4.2248	y_{176}	0.2678	0.00081
4.3412	y_{177}	0.2784	0.00084

Table 4: Difference between perturbed and unperturbed solution, $k_0 = 32, 64, N = 256, \Delta t = 0.00194$

6 Large scale forcing

In this section we discuss whether the large scale determines the small scale. We start with a large scale experiment of type 1) from section 1. We choose $k_c = 12$, and solve the equations (1.1) with initial data (1.4). Norms of the difference $\xi_b^y - \xi_T^y$ can be found in table 5 and a contour plot in figure 11. It is clear, at least for the simulation time considered here, that the small scales are not reproduced.

For the large scale experiment of type 2) we make three calculations with $k_c = 8, 10, 12$, respectively to determine $\boldsymbol{u}_{pb}^{II}(\boldsymbol{x}, t)$ from the time history of $\boldsymbol{u}_b^I(\boldsymbol{x}, t)$. Thus, we solve (1.6) with

$$\boldsymbol{u}^I(\boldsymbol{x}, t) = \boldsymbol{u}_b^I(\boldsymbol{x}, t),$$

and the initial data

$$\boldsymbol{u}^{II}(\boldsymbol{x}, 0.5) = 0.$$

In figure 12 and figure 13, contour plots of ξ_b^y and of ξ_{pb}^y for $k_c = 8$ are shown for $t = 0.5, 2.36$ respectively in $y = const.$ planes. The same plane is chosen for the playback-runs as for the base-run-2, which as before is chosen as the plane for which the maximum of $|\xi_b^y|$ is attained (at the time t of consideration). Contours of the difference $\xi_b^y - \xi_{pb}^y$ at $t = 2.36$ are plotted in figure 14. In figure 15 to figure 20, corresponding contour plots for $k_c = 10, 12$ are shown. The difference for $k_c = 8, t = 2.36$ is rather big. For $k_c = 10, 12$, the match is much better and all structures visible in the base-run-2 are also present in the playback-runs. L_2 norm and max norm estimates also reveal this, c.f. table 6.

In figure 21, the spectrum of the base-run-2 is plotted in a log-log diagram at some times t. Also the relative difference of spectrum between the base-run-2 and the playback-runs are shown, i.e.

$$(E_b(k) - E_{pb}(k))/E_b(k),$$

where E_b, E_{pb} are the spectrums of the base-run-2 and the playback-runs respectively. Note that by definition this relative difference of the spectrum, at $t = 0.5$ is zero for the large scale and one for small scale. During the time interval of the calculation, the relative difference diminishes for all small scales and for all $k_c = 8, 10, 12$.

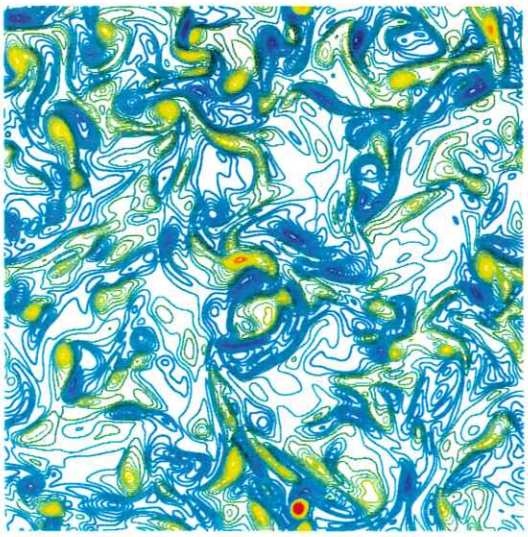

(a) (min,max): $(-17.8, 27.0)$

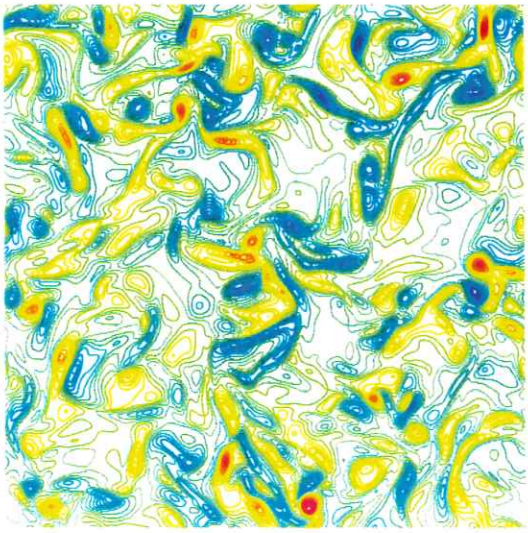

(b) (min,max): $(-19.6, 20.0)$

Figure 11: Contour plots of the y component of the vorticity, base-run-2 (a) and truncate-run (b), $t = 2.36, y = y_{193}$. Contour spacing:1

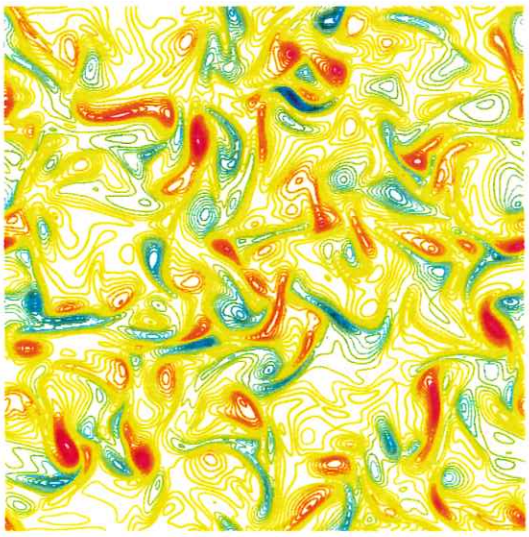

(a) (min,max): $(-30.3, 19.8)$

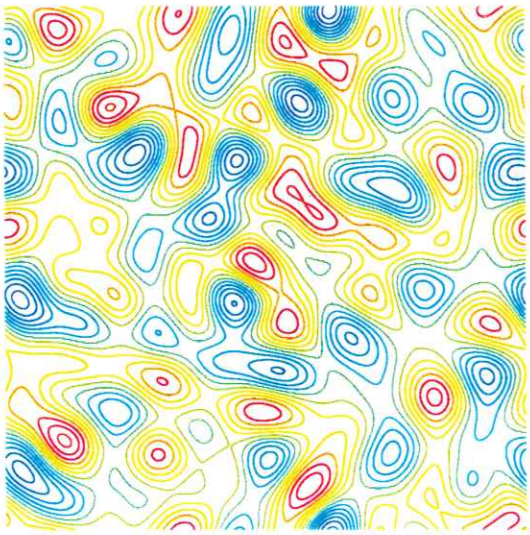

(b) (min,max): $(-7.6, 6.3)$

Figure 12: Contour plots of the y component of the vorticity, base-run-2 (a) and playback-8 (b), $t = 0.5, y = y_{264}$. Contour spacing:1

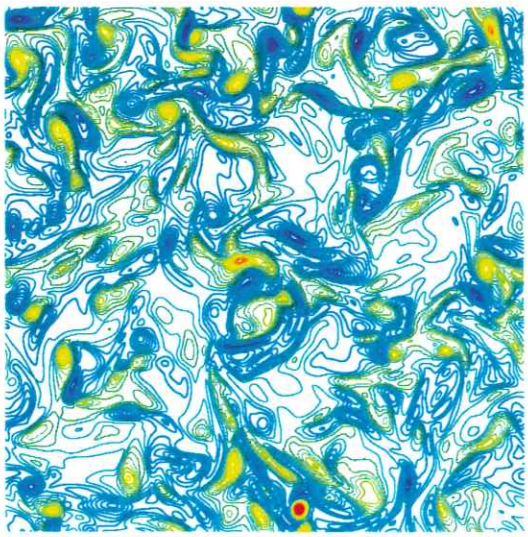

(a) (min,max): $(-17.8, 27.0)$

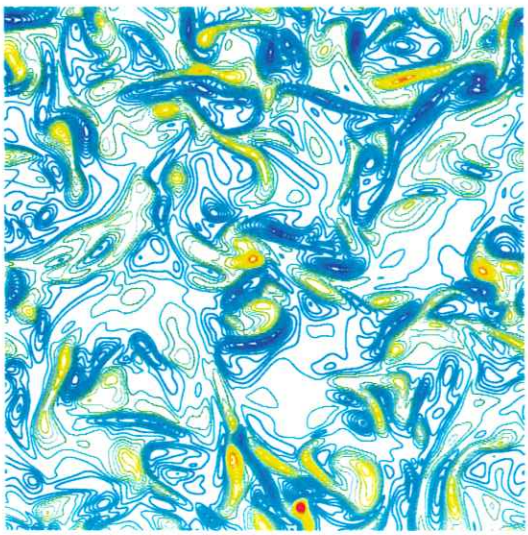

(b) (min,max): $(-14.3, 21.6)$

Figure 13: Contour plots of the y component of the vorticity, base-run-2 (a) and playback-8 (b), $t = 2.36, y = y_{193}$. Contour spacing:1

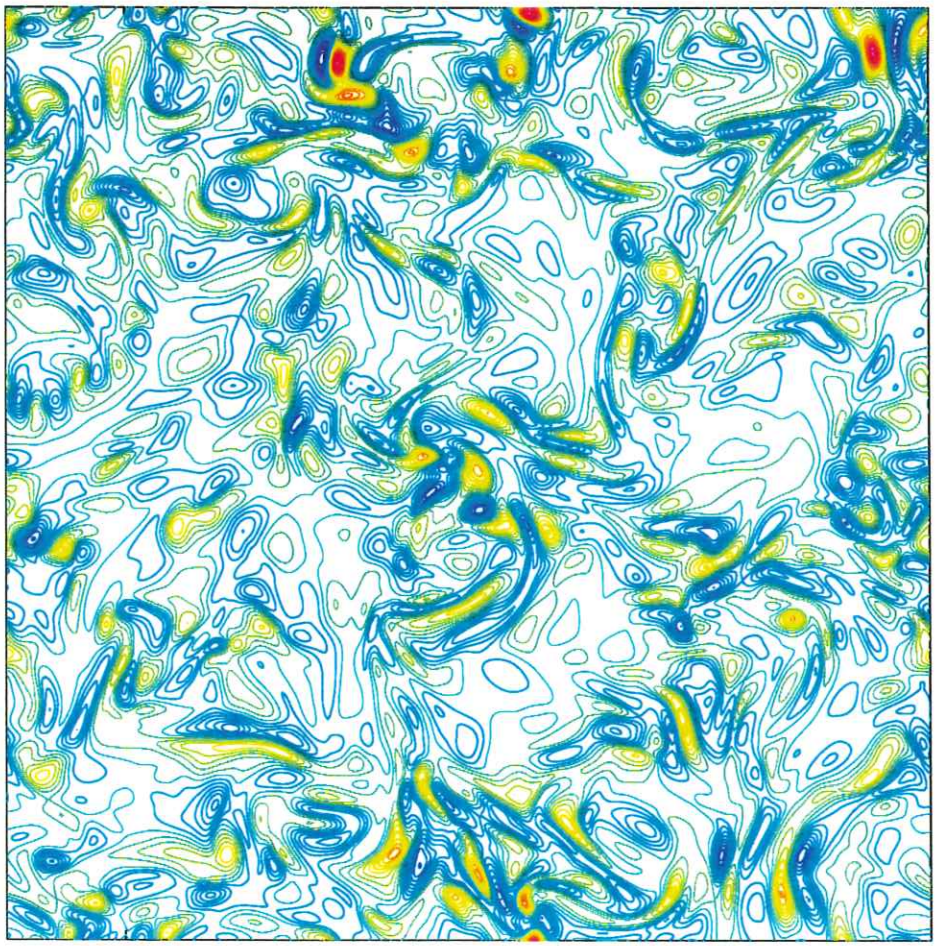

Figure 14: Difference between base-run-2 and solution to forced equations: $\xi_b^y - \xi_8^y$ at $y = y_{193}, t = 2.36$. Contour spacing:1, (min,max):$(-12.0, 16.5)$

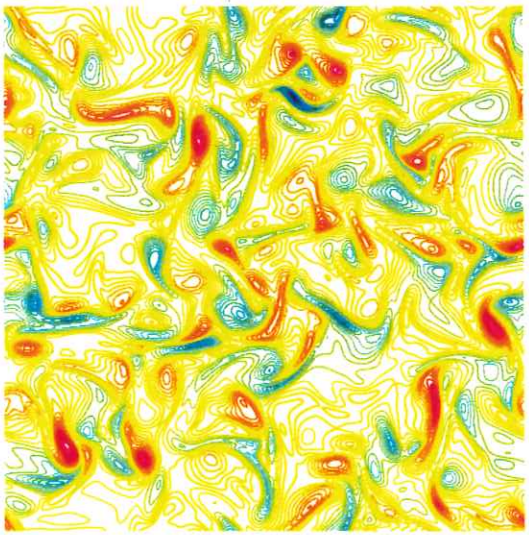

(a) (min,max): $(-30.3, 19.8)$

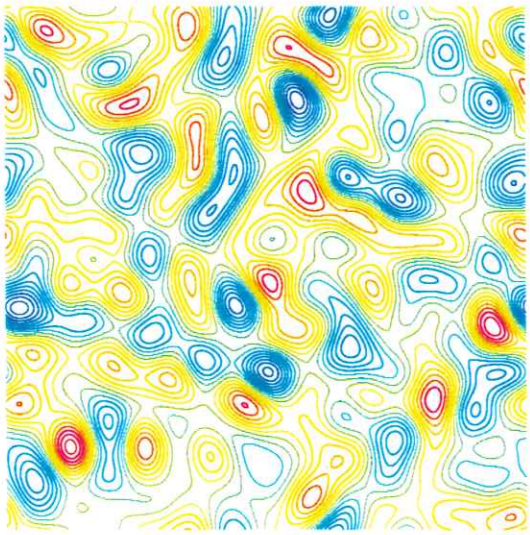

(b) (min,max): $(-9.7, 8.6)$

Figure 15: Contour plots of the y component of the vorticity, base-run-2 (a) and playback-10 (b), $t = 0.5, y = y_{264}$. Contour spacing:1

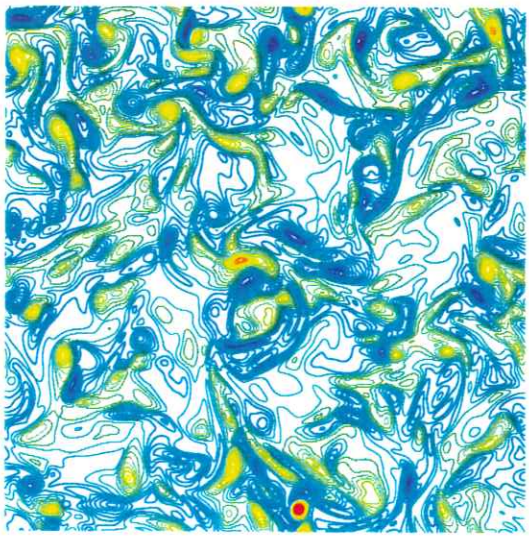

(a) (min,max): $(-17.8, 27.0)$

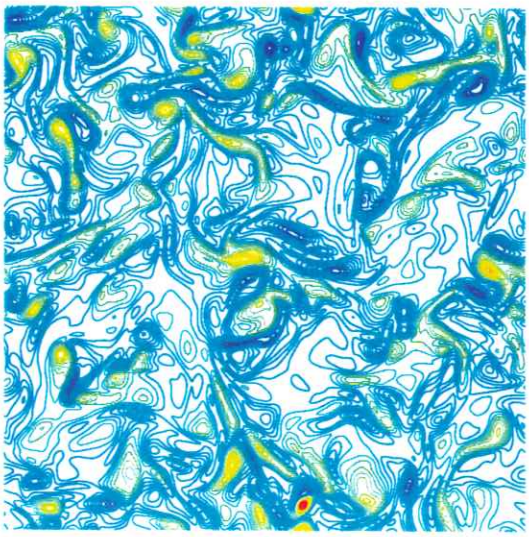

(b) (min,max): $(-15.9, 26.1)$

Figure 16: Contour plots of the y component of the vorticity, base-run-2 (a) and playback-10 (b), $t = 2.36, y = y_{193}$. Contour spacing:1

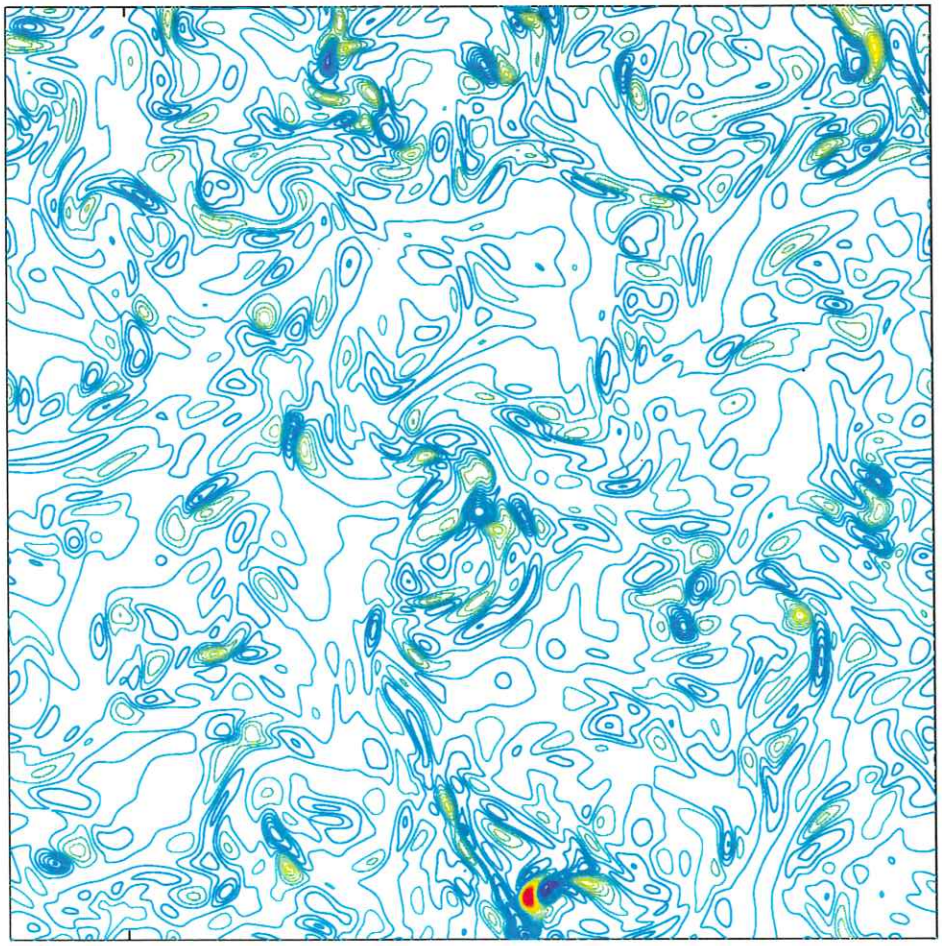

Figure 17: Difference between base-run-2 and solution to forced equations: $\xi_b^y - \xi_{10}^y$ at $y = y_{193}, t = 2.36$. Contour spacing:1, (min,max):$(-14.6, 22.6)$

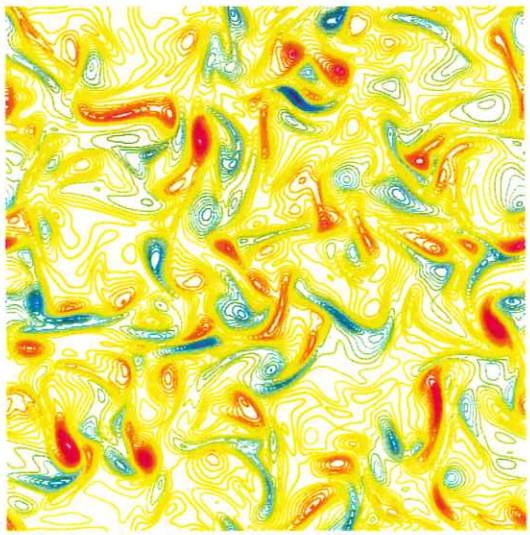

(a) (min,max): $(-30.3, 19.8)$

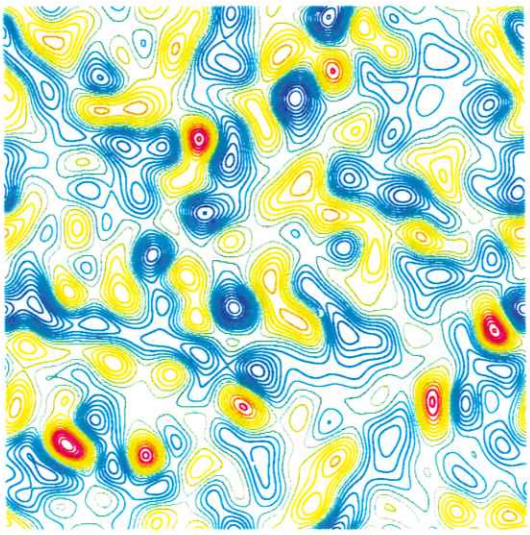

(b) (min,max): $(-9.8, 11.8)$

Figure 18: Contour plots of the y component of the vorticity, base-run-2 (a) and playback-12 (b), $t = 0.5, y = y_{193}$. Contour spacing:1

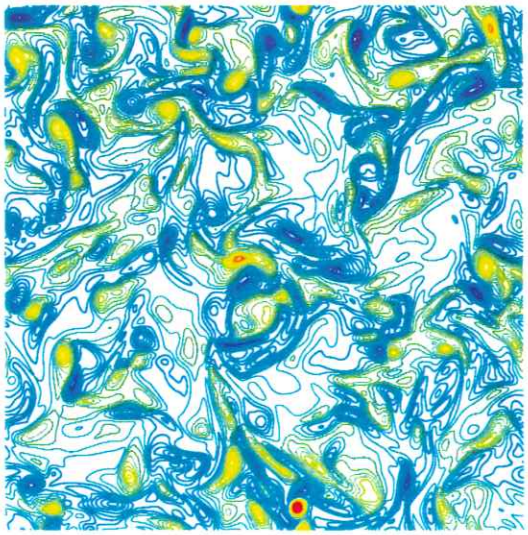

(a) (min,max): $(-17.8, 27.0)$

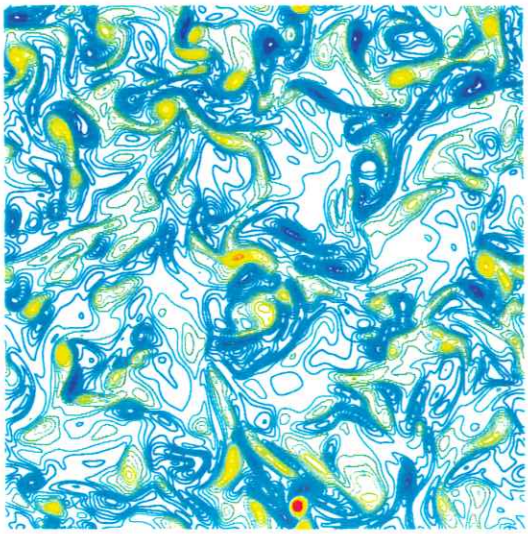

(b) (min,max): $(-16.8, 25.0)$

Figure 19: Contour plots of the y component of the vorticity, base-run-2 (a) and playback-12 (b), $t = 2.36, y = y_{193}$. Contour spacing:1

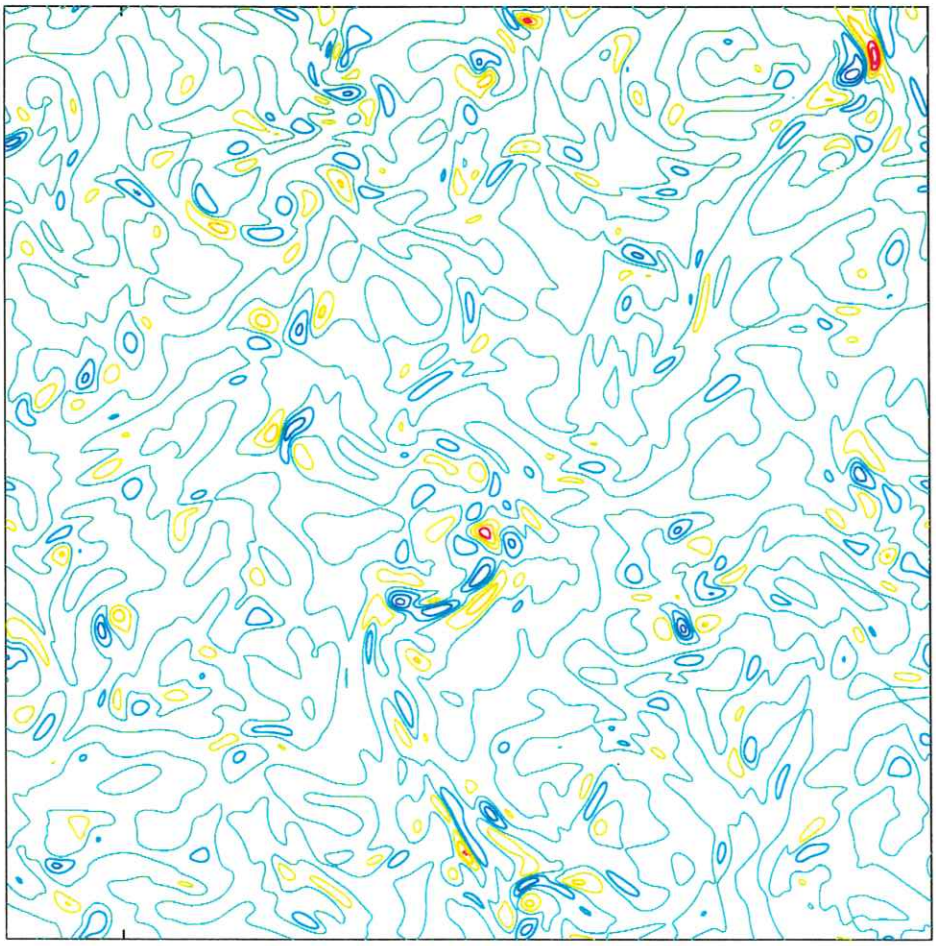

Figure 20: Difference between base-run-2 and solution to forced equations: $\xi_b^y - \xi_{12}^y$ at $y = y_{193}, t = 2.36$. Contour spacing:1, (min,max):$(-3.6, 4.6)$

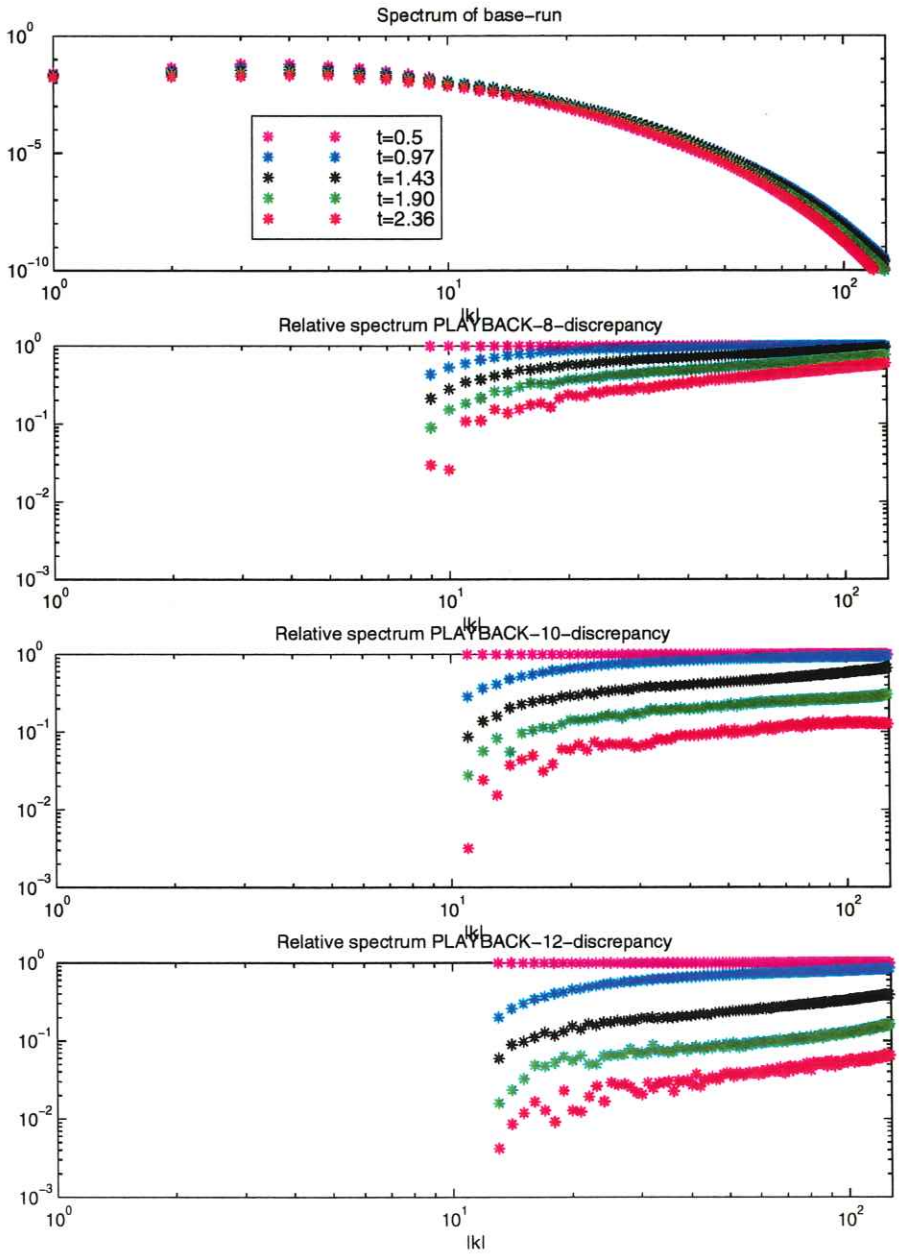

Figure 21: Relative difference of the spectrum, for 8,10, and 12 mode forcing

t	y	$\frac{\|\xi_b^y - \xi_T^y\|^2}{\|\xi_b^y\|^2}$	$\frac{\|\xi_b^y - \xi_T^y\|_{max}}{\|\xi_b^y\|_{max}}$
0.50	y_{264}	0.316	0.6794
0.97	y_{263}	0.228	0.6542
1.43	y_{193}	0.345	0.8749
1.90	y_{189}	0.553	1.0399
2.36	y_{193}	0.664	0.9513
2.83	y_{153}	0.972	0.9018
3.29	y_{149}	1.20	1.0608
3.76	y_{171}	1.34	1.0051
4.22	y_{176}	1.47	0.9552

Table 5: Relative norms of the difference of the y-component of vorticity, between base-run-2 and the truncate-run.

Acknowledgment

We would like to thank Dr. Richard Lau at the Office of Naval Research for all the support he has given us over the years. We would like to thank Prof. Arne Johansson for letting us use their computer program and PhD student Krister Alvelius for helping us get started with the code, both at the Department of Mechanics at the Royal Inst. of Technology in Stockholm Sweden. We gladly acknowledge many stimulating discussions with Dr. William Henshaw at Los Alamos National Laboratory and Dr. Gerald Browning at CIRA, Colorado State University and NOAA Forecast System Laboratory. All calculations presented here are done at the DoD High Performance Computing Center, Naval Oceanographic Office(NAVO) MSRC on their Cray C916 PVP system. The post processing is done with ©Matlab v5.1.

References

[1] W.D. Henshaw, H.-O. Kreiss, and L.G. Reyna. On the smallest scale for the incompressible navier-stokes equations. *Theoretical and Computational Fluid Dynamics*, 1:65–95, 1989.

k_c	t	y	$\frac{\|\xi_b^y - \xi_{pb}^y\|^2}{\|\xi_b^y\|^2}$	$\frac{\|\xi_b^y - \xi_{pb}^y\|_{max}}{\|\xi_b^y\|_{max}}$
8	0.50	y_{264}	0.551	0.8020
8	0.97	y_{263}	0.496	0.8358
8	1.43	y_{193}	0.460	0.6511
8	1.90	y_{189}	0.450	0.8655
8	2.36	y_{193}	0.475	0.6114
10	0.50	y_{264}	0.430	0.7165
10	0.97	y_{263}	0.314	0.7839
10	1.43	y_{193}	0.234	0.6549
10	1.90	y_{189}	0.207	1.0202
10	2.36	y_{193}	0.150	0.8389
10	2.83	y_{153}	0.140	0.4635
10	3.29	y_{149}	0.099	0.3006
10	3.76	y_{171}	0.075	0.2971
10	4.22	y_{176}	0.053	0.2303
12	0.50	y_{264}	0.316	0.6794
12	0.97	y_{263}	0.168	0.6588
12	1.43	y_{193}	0.083	0.2881
12	1.90	y_{189}	0.050	0.2373
12	2.36	y_{193}	0.0319	0.1711
12	2.83	y_{153}	0.0221	0.1566
12	3.29	y_{149}	0.0111	0.1097
12	3.76	y_{171}	0.0070	0.1272
12	4.22	y_{176}	0.0038	0.0626

Table 6: Relative norms of the difference of the y-component of vorticity, between base-run-2 and the playback-runs.

[2] W.D. Henshaw and H.-O. Kreiss. A numerical study of the propagation of perturbations in the solution of the 2d incompressible navier-stokes equations. Technical Report RC 16251 (#72137) 11/1/90, IBM Research Division, T.J.Watson Research Center Yorktown Heights, NY 10598, also in the proceedings for the Third International Conference on Hyperbolic Problems, Uppsala University, 1990.

[3] G.L. Browning, W.D. Henshaw, and H.-O. Kreiss. A numerical investigation of the interaction between the large and small scales of the two-dimensional incompressible navier-stokes equations. Technical Report CAM 98-23, Department of Mathematics, UCLA, Los Angeles, CA 90024, USA, 1998.

[4] A. Lundbladh, D.S. Henningson, and A.V. Johansson. An efficient spectral integration method for the solution of the navier-stokes equations. Technical Report FFA-TN 1992-28, The Aeronautical Research Institute of Sweden, 1992.

[5] M. Hallbäck. Development and critical evaluation of turbulent models through direct numerical simulation of homogeneous turbulence. Technical Report TRITA-MEK 1993:2, Department of Mechanics, Royal Institute of Technology, Sweden, 1993.

[6] K. Alvelius. Large eddy simulations of homogeneous turbulence. Technical Report TRITA-MEK 1997:12, Department of Mechanics, Royal Institute of Technology, Sweden, 1997.